# A STUDY OF WING BODY BLENDING FOR AN

## ADVANCED SUPERSONIC TRANSPORT*

T.P. Goebel, E. Bonner, and D.A. Robinson
North American Aircraft Division
Rockwell International

## SUMMARY

Increases in supersonic cruise lift-drag ratio were sought at Mach numbers 2.2 and 2.7 using wing-body planform and thickness blending. Constrained twist and camber optimization was performed in the presence of nacelles. Wing and fuselage thickness distributions were optimized for either minimum volume wave drag or minimum total pressure wave drag. The zero leading edge suction lift drag ratios were determined for three wing planforms. The magnitude of the effect of leading edge suction on attainable lift drag ratio was defined on one planform and an estimation of available leading edge suction was made.

## INTRODUCTION

A variety of configuration arrangements have been considered for large supersonic cruising aircraft in past NASA and industry studies. Many early arrangements are described in a 1967 NASA summary and index of experimental characteristics (ref. 1). One promising configuration has been used as a focus for recent AST-100, 105-1, and 200 studies (refs. 2-4). This arrangement employs a highly swept wing of moderate taper ratio, underslung nacelles, an aft-fuselage-mounted horizontal tail surface and fuselage-and-wing-mounted vertical surfaces. The present study uses this arrangement as a starting point and defines improvements due to wing-body blending. A resized AST-100, designated the AST-102, was selected as the Mach 2.7 baseline configuration. The objective of the present study is to evaluate the effect of wing-body blending on the performance of a supersonic cruising aircraft. The approach, as shown on figure 1, emphasizes the aerodynamic design tools available at Rockwell and which differ from those available elsewhere in the industry.

| | |
|---|---|
| C | chord, m |
| $C_D$ | drag coefficient |
| $C_L$ | lift coefficient |
| D | drag, N |
| L | lift, N |
| q | dynamic pressure, $N/m^2$ |
| S | leading edge suction parameter |
| $S_W$ or $S_{REF}$ | reference wing area, $m^2$ |
| t | thickness, m |
| x,y,z | cartesian coordinates, m |
| $\beta$ | $\sqrt{M^2-1}$ |
| $\eta$ | nondimensional spanwise coordinate |
| $\Lambda$ | sweepback angle, deg |
| $\theta$ | roll angle, deg |

Subscripts:

| | |
|---|---|
| c.g. | center of gravity |
| C.P. | center of pressure |
| F | friction |
| L | lifting |
| LE | leading edge |
| TE | trailing edge |
| W | wave drag |

## PLANFORM SELECTION

The AST-102 leading edge has three straight line segments with sweepback angles of 74, 71 and 60 degrees. The Rockwell blended RB-1 leading edge has, except for an inboard modification, two straight line segments with sweepback angles of 74 and 68.5 degrees, figure 2. The inboard leading-edge modification was made to facilitate blending. Increased outboard leading-edge sweep was used to achieve a higher supersonic cruise lift-to-drag (L/D) ratio and is consistent with an earlier design integration study (ref. 5). An outboard leading edge sweep of 68.5 degrees was selected as the highest for which acceptable low speed characteristics could be expected at landing angles up to 8 to 10 degrees. A leading edge sweep increase to 72.3 degrees would be required at M = 2.7 to satisfy the recently developed Carlson suction criteria $\beta$ cot $\Lambda_{LE} \leq 0.8$. The inboard trailing edge was kept identical to the AST-102 because good low speed flap effectiveness requires low trailing edge sweep. The outboard trailing edge sweep was increased, however, from 41.5 degrees on the AST-102 to 45.4 degrees on the RB-1 to allow sufficient outboard chord for leading and trailing edge devices. With these planform modifications and after application of the aerodynamic design codes, the blended configuration indicated on figure 3 evolved.

## TWIST AND CAMBER OPTIMIZATION

Two linear optimizers are available for use with a swept panel analysis program (ref. 6). All three solvers can treat the wing, fuselage, and horizontal and vertical surfaces as twisted and cambered surfaces within the frame work of linearized flow theory. The analysis program can represent several fuselage and nacelle shaped bodies as slender bodies.

12 spanwise and 10 chordwise wing panels and 1 spanwise and 20 chordwise fuselage panels were used in all three programs. In the analysis program, rectangular shells were placed around circular slender-body nacelles, figure 4. 10 chordwise and 4 wrap-around panels were used on the rectangular shells. The function of the shells is to provide surfaces for matching boundary conditions between the slender body nacelle solutions and cambered and twisted surface solutions.

Due to differing capabilities of the available computer programs, the twist and camber design cycle required several steps, figure 5. In step A the wing is represented as a thin cambered and twisted surface and the fuselage as a cambered plate. The basic design program produces the optimum twist and camber of the wing and fuselage for a specific lift and moment constraint.

In step B this twist and camber are evaluated in the analysis program with nacelles present. In step C the design is refined with the nacelle upwash from step B added at the control points of those wing panels influenced by the nacelles. In step D the analysis program was used to evaluate the revised optimum twist and camber with nacelles on. In step E the auxiliary design program was used to establish the changes in twist and camber to cancel the wing pressure differences between steps C and D. The blended wing-body-nacelle design achieved a lifting efficiency level within 2% of the wing alone case and is equivalent to an arrow wing of the same sweep and aspect ratio with a notch ratio of 0.4 (see figure 14 of reference 5). The final twist and camber distribution was evaluated in the analysis program across the Mach number range to obtain trimmed drag due to lift for 0% and 100% leading edge suction (L.E.S.) condition. The M = 2.7 design twist and camber for the blended planform at $C_L$ = 0.1 is presented on figures 6 through 9.

## WING-FUSELAGE VOLUME OPTIMIZATION

An analysis program is available to calculate supersonic volume and lift-volume wave drag. The spatial singularities which are solutions to the linearized equations of motion are reduced to a series of equivalent lineal distributions by application of the cutting (oblique) plane concept. The drag is calculated using slender body theory (refs. 7 and 8). The total wave drag includes volume, angle of attack, twist and camber, and lift-volume interference effects. In the analysis mode, the wave drag is evaluated using 13 roll angles and 50 longitudinal cuts.

For wing and fuselage thickness optimization, a design solver is used to minimize either volume wave drag or total wave drag subject to specific volume and local thickness constraints. The physical geometry is perturbed by a set of harmonic functions. Lagrange's method for extremal problems with constraints is applied to the expression for wave drag. A set of linear equations is solved for the perturbation coefficients that minimize the drag. In the design mode, the wave drag is evaluated using 5 roll angles and 50 longitudinal cuts.

In an application of the volume wave drag option with a fixed wing-body volume of 1139.5 $m^3$, the volume wave drag (5 roll angles) was reduced from D/q = 1.501 to 1.370 $m^2$, figure 10. In this case, 13 thickness constraints were used. The resulting fuselage and wing sections are shown on figure 11 and the volume wave drag versus Mach number on figure 12. The wing and fuselage were treated as a single wing-like component. When the components were treated separately, the lowest $C_{D_W}$ value obtained by successive optimizations of the fuselage and wing was 0.002044 compared to the 0.001765 value of figure 10.

In an application of the total wave drag option with a fixed wing body volume of 1009.9 $m^3$, the total pressure wave drag (5 $\theta$) was reduced at $C_L$ = 0.1 from D/q = 2.652 to 2.521 $m^2$, figure 13. Fourteen (14) thickness constraints were used for this case. The resulting fuselage and wing sections are shown on figure 14. With either option, the optimizer reduced the thickness ratio of wing sections to the minimum allowed (0.025) just outboard of the wing fuselage juncture at $\eta$ = 0.0835.

## LOWER BOUND DRAG

The 100% leading edge suction airplane drag is obtained from predictions of wave drag due to volume and lift, and vortex drag. The 100% suction drag due to lift is evaluated from this information as follows

$$C_{D_L}(100\% \text{ LES}) = C_{D_{WAVE \text{ } LIFT+VOL}} - C_{D_{WAVE \text{ } VOL}} + C_{D_{VORTEX}}$$

An alternative estimation procedure is to evaluate the strength of the leading edge singularity from calculated chordwise net pressure distributions. These independent predictions of drag-due-to-lift are compared on figure 15. The analysis program calculation of the 0% LES drag due to lift is considered more accurate due to inclusion of nacelle effects. The far field evaluation of the 100% suction drag due to lift is regarded as more accurate based on comparison with exact conical solution for delta wings.

## LEADING EDGE SUCTION ESTIMATION

A correlation was made of available low speed supersonic transport data on leading edge suction. The framework for the correlation used 0% and 100% LES curves for a cambered and twisted plate calculated by a variant of the analysis program discussed earlier (ref. 6). The leading edge suction parameter S has the value 0.0 at 0% LES and 1.0 at 100% LES. With leading and trailing edge flaps undeflected and based on wind tunnel data in the freestream Reynolds number $(R_{e_{\bar{c}}})$ range 2.5 x $10^6$ to 13.6 x $10^6$, correlated S values of 0.3 to 0.4 were obtained. With leading edge flaps deflected and based on data in the freestream Reynolds number range 2.5 x $10^6$ to 6.0 x $10^6$, correlated S values approaching 0.9 were obtained. The low speed S value variation with $C_L$ is indicated by the symbols at Mach number 0.2 on figure 16. Full scale freestream Reynolds number based on $\bar{c}$ is 1.3 x $10^8$ at Mach number 0.2.

Exploratory calculations were made at higher speeds using the Carlson-Mack LES correlation (ref. 9) and leading edge radii at span stations $\eta$ = 0.15 and 0.70 on the RB-1 wing for lift coefficients of 0.1 and 0.25. This correlation uses chords and leading edge radii on sections normal to the leading edge. Correlated data shown (ref. 9) are in the normal Reynolds number ($Re_{c_n}$) range 0.4 x $10^6$ to 6.0 x $10^6$. With leading and trailing edge flaps undeflected, S values are shown on figure 16 for $C_L$ = 0.25 at Mach number 0.9 and 2.7 and for $C_L$ = 0.1 at Mach number 2.7. These point values fall above and below the integrated correlated curves. Full scale normal Reynolds numbers are in the range 0.6 to 2.6 x $10^8$.

In either of these correlations, the extrapolation with Reynolds numbers from the wind tunnel data base to full scale is from $10^6$ to $10^8$ or two orders of magnitude.

Estimated S values based on these correlations are shown as solid lines on figure 16 and were used to obtain the estimated drag due to lift curves shown as dashed curves on figures 17, 18, and 19 and versus Mach number on figure 20.

DESIGN STATUS

Nacelles were integrated into the RB-1 configuration with a drag penalty of roughly 77% of the nacelle skin friction drag, figure 21.

Several different 0% LES comparisons have been made with the AST-102 baseline, figure 22. In the first, the geometry was provided by NASA and the AST-102 was analyzed by Rockwell analysis codes. Results are the first line of numbers shown on figure 22. The drag due to lift value $C_{D_L}$ is suspect since the analysis program does not reproduce design results when geometry is transferred as ordinates rather than slopes. The twist constrained basic design program was run on the AST-102 planform to obtain $C_{D_L}$ = 0.004202, step A on figure 5. The difference between steps A and F was added to give an approximate nacelle integration penalty. Results are the second line of numbers on figure 22. An NASA/Langley AST-102 analysis was obtained at M = 2.62 and was adjusted to M = 2.7. Results are the third line of numbers on figure 22. The fairest comparison to show the effect of blending is considered to be between 0% LES L/D values of 9.614 and 9.234 or a benefit of 0.380 over the AST-102 baseline.

The 0% and 100% LES design status is summarized on figure 23. The 0% LES wing body was optimized for minimum volume wave drag. The 100% LES wing body was optimized for minimum lift-volume wave drag. Based on an estimated LES

154

attainable of 66%, an L/D of 10.20 is indicated at the design point. The corresponding complete trimmed drag polar is presented on figure 24.

Part of the study was a task to design a Mach number 2.2 configuration. Related to this task 0% LES analyses were carried through at Mach number 2.2 on three planforms, figure 25. 0% LES comparisons are summarized on figure 26. Geometry and data to obtain $C_{DL}$ for the D-77 baseline were taken from a wind tunnel data report (ref. 10). Rockwell analysis codes gave the results shown on the first line of numbers on figure 26. The twist constrained basic design program was run on the D-77 planform to obtain $C_{DL}$ = 0.003943 at M = 2.2, step A on figure 5. The difference between step A and F for a M = 2.2 analysis on the RB-1 was added to give an approximate nacelle integration penalty on the D-77. The wing body volume was redistributed subject to thickness constraints to minimize volume wave drag. Results are the second line of numbers on figure 26. The twist constrained basic design program was, again, rerun on the AST-102 planform to obtain $C_{DL}$ = 0.003276 at M = 2.2. Again the difference between steps A and F for an M = 2.2 RB-1 was added to give an approximate nacelle integration increment. The effects of blending at M = 2.2 were an 0.326 increase in 0% LES L/D over the AST-102 baseline and a 1.186 increase over the D-77 baseline.

CONCLUSIONS

1) Although planform compromises to insure good low speed characteristics tend to make achievement of high supersonic efficiency difficult, cruise L/D ratios of approximately 10.0 appear possible at a Mach number of 2.7 for a blended configuration. Careful attention must be given to wing twist and camber, wing fuselage thickness distributions, nacelle integrations, and wing leading edge suction attainment.

2) Improved determination of leading edge suction attainable at Reynolds numbers two orders of magnitude higher than covered in available published data would reduce the uncertainty of supersonic L/D estimates.

REFERENCES

1. Ray, E. J.: NASA Supersonic Commercial Air Transport (SCAT) Configuration: A Summary and Index of Experimental Characteristics. NASA TM X-1329, Jan. 1967.

2. Baber, H. T., Jr. and Swanson, E. E.: Advanced Supersonic Technology Concept AST-100 Characteristics Developed in a Baseline-Update Study. NASA TM X-72815, Jan. 1976.

3. Baber, H. T., Jr.: Characteristics of the Advanced Supersonic Technology AST-105-1 Configured for Transpacific Range with Pratt and Whitney Aircraft Variable Stream Control Engines. NASA TM-78818, March 1979.

4. Walkley, K. B. and Martin, G. L.: Aerodynamic Design and Analysis of the AST-200 Supersonic Transport Configuration Concept. NASA CR-159051, April 1979.

5. Baals, D. D., Robins, A. W. and Harris, R. V., Jr.: Aerodynamic Design Integration of Supersonic Aircraft. AIAA Paper 68-1018, 1968.

6. Bonner, E., Clever, W. and Dunn, K.: Aerodynamic Preliminary Analysis System Part I - Theory. NASA CR-145284, April 1978.

7. Bonner, E.: The Expanding Role of Potential Theory in the Design of Supersonic Aircraft. Jour. of Aircraft, vol. 8, no. 5, May 1971, pp. 347-353.

8. Lomax, H.: The Wave Drag of Arbitrary Configurations in Linearized Flow as Determined by Areas and Forces in Oblique Planes. NACA RM A55A18, 1955.

9. Carlson, H. W., Mack, R. J. and Barger, R. L.: Estimation of Attainable Leading-Edge Thrust. NASA TP 1500, 1979.

10. Radkey, R. L., Welge, H. R. and Felix, J. E.: Aerodynamic Characteristics of a Mach 2.2 Advanced Supersonic Cruise Aircraft Configuration at Mach Numbers from 0.5 to 2.4. NASA CR-145094, Feb. 1977.

● OBJECTIVE

    - IMPROVE SUPERSONIC CRUISE PERFORMANCE

● APPROACH

    - LINEAR AERODYNAMIC OPTIMIZATIONS AT M = 2.7 AND $C_L$ = 0.10

        DRAG DUE TO LIFT AND CAMBER

            ROCKWELL DESIGN CODE BASED ON WOODWARD
            FINITE ELEMENT

        VOLUME WAVE DRAG AND TOTAL PRESSURE DRAG
            ROCKWELL MODAL DESIGN CODES

Figure 1.- Blended wing body study.
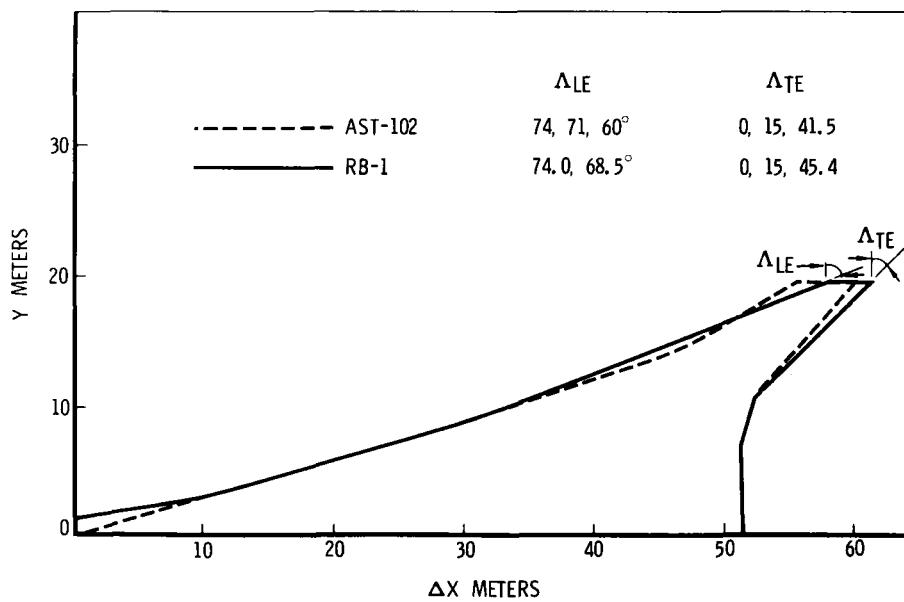


Figure 2.- Planform comparison.
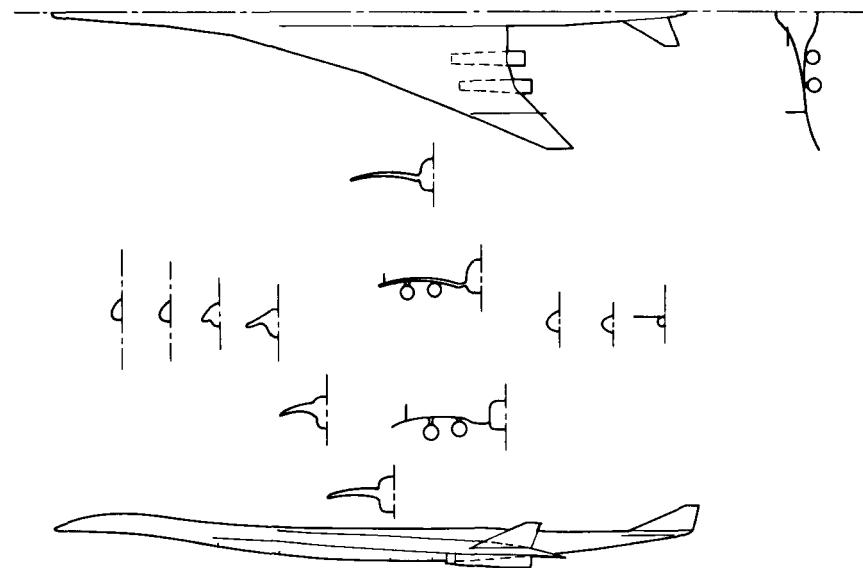
Figure 3.- Blended configuration - RB-1.

NACELLES

NACELLE SHELLS

WING PANELS
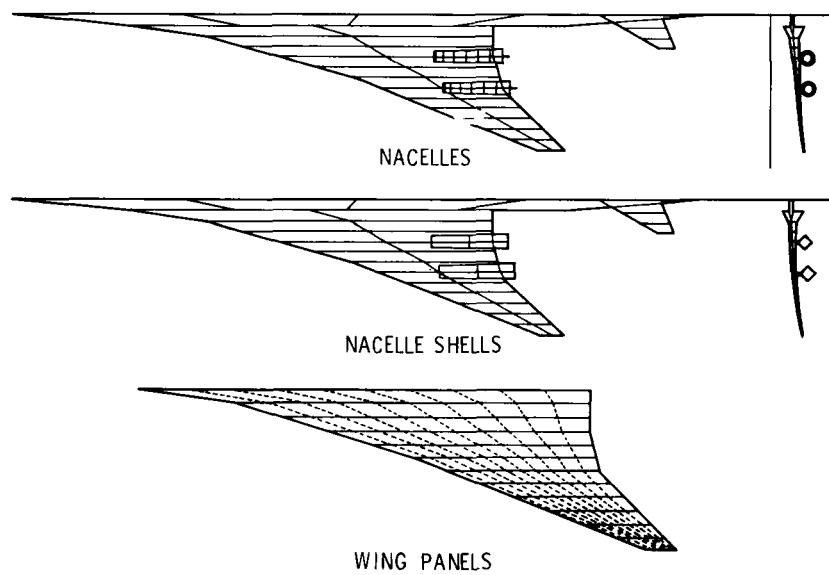
Figure 4.- Twist and camber theoretical models.

$\Delta C_{D_L}^{*}$

A  BASIC DESIGN PROGRAM (NACELLES OFF)

       TWIST CONSTRAINED NEAR PLANFORM DISCONTINUITY    0.004066

B  ANALYSIS PROGRAM (NACELLES ON)    0.004276

C  AUXILIARY DESIGN PROGRAM (NACELLES OFF)

       NACELLE UPWASH FROM B    0.004080

D  ANALYSIS PROGRAM (NACELLES ON)    0.004300

E  INCREMENT IN TWIST AND CAMBER TO CANCEL PRESSURE
   DIFFERENCE BETWEEN C AND D

F  ANALYSIS PROGRAM (NACELLES ON)    0.004146

*ZERO SUCTION, $S_{REF}$ = 784.8 $m^2$

Figure 5.- Twist and camber design cycle steps — M = 2.7, $C_L$ = 0.1.
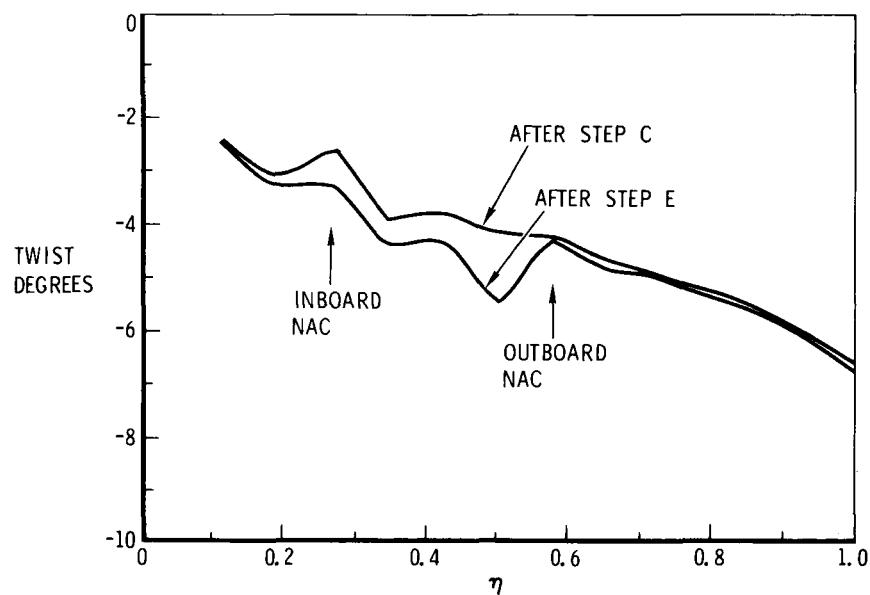


Figure 6.- Design twist — M = 2.7, $C_L$ = 0.1.
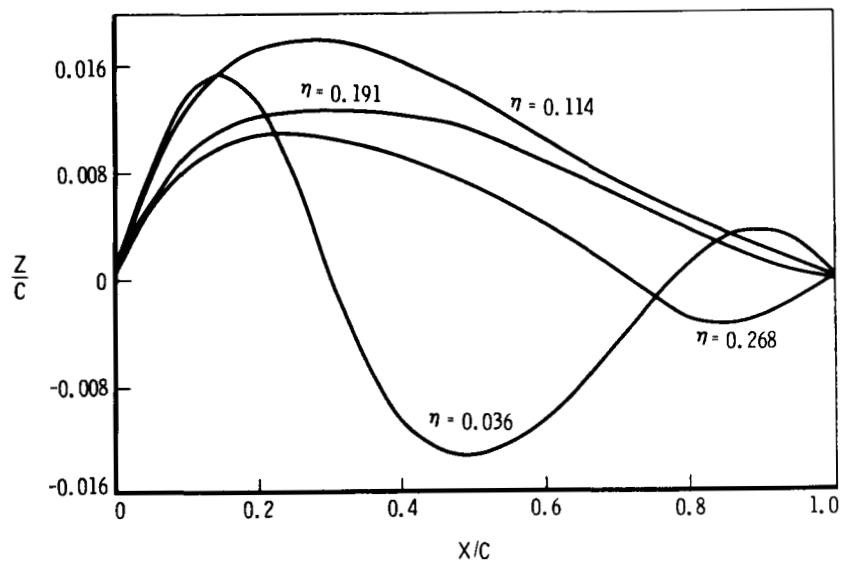
Figure 7.- Design camber — M = 2.7,  $C_L$ = 0.1.
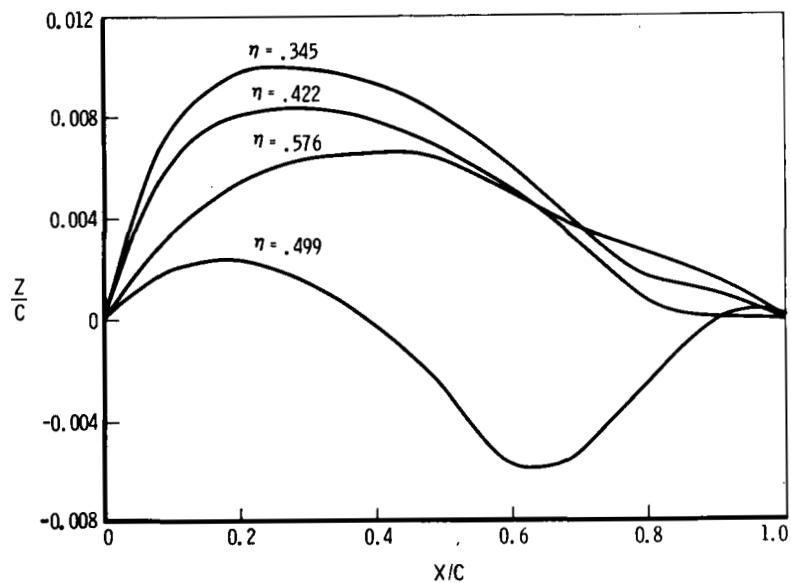


Figure 8.- Design camber — M = 2.7,  $C_L$ = 0.1.
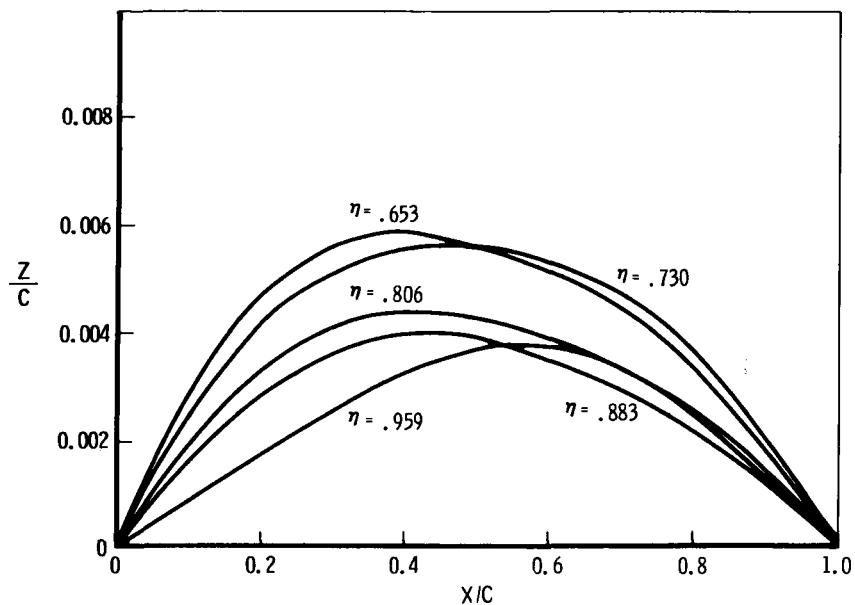
Figure 9.- Design camber — M = 2.7, $C_L$ = 0.1.

CONSTRAINTS

| $\eta$ | X/C |
|---|---|
| 0.0000 | 0.2, 0.8 |
| 0.0405 | |
| 0.0788 | 0.4 |
| 0.0835 | 0.4, 0.8 |
| 0.1538 | 0.4 |
| 0.2308 | 0.4 |
| 0.3077 | 0.4 |
| 0.4615 | 0.4 |
| 0.5385 | 0.4 |
| 0.6154 | |
| 0.6923 | 0.4 |
| 0.8462 | 0.4 |
| 1.0000 | 0.4 |

| D/Q M$^2$ | OPT D/Q M$^2$ | | $\Delta c_{D_W}$ |
|---|---|---|---|
| 1.501 | 1.370 | (5 $\Theta$) | 0.001745 |
| | 1.385 | (13 $\Theta$) | 0.001765 |

Figure 10.- Wave drag optimization — M = 2.7, $VOL_{WB}$ = 1139.5 m$^3$.

$\eta = 0.0$  T/C = .058

$\eta = .1538$  T/C = .026

$\eta = .0405$  T/C = .071

$\eta = .4615$  T/C = .026

$\eta = .0788$  T/C = .050

$\eta = .8462$  T/C = .025

$\eta = .0835$  T/C = .025
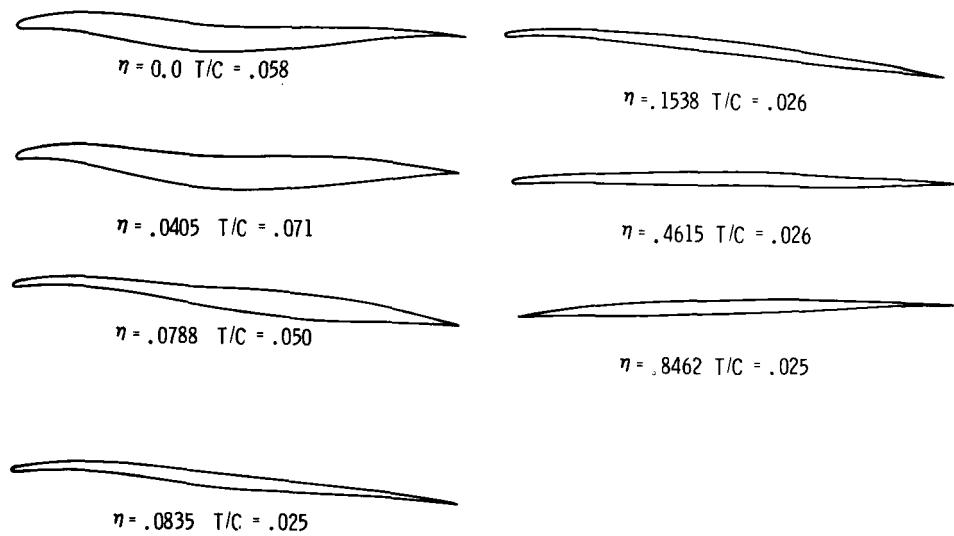
Figure 11.- Sections for minimum wave drag.
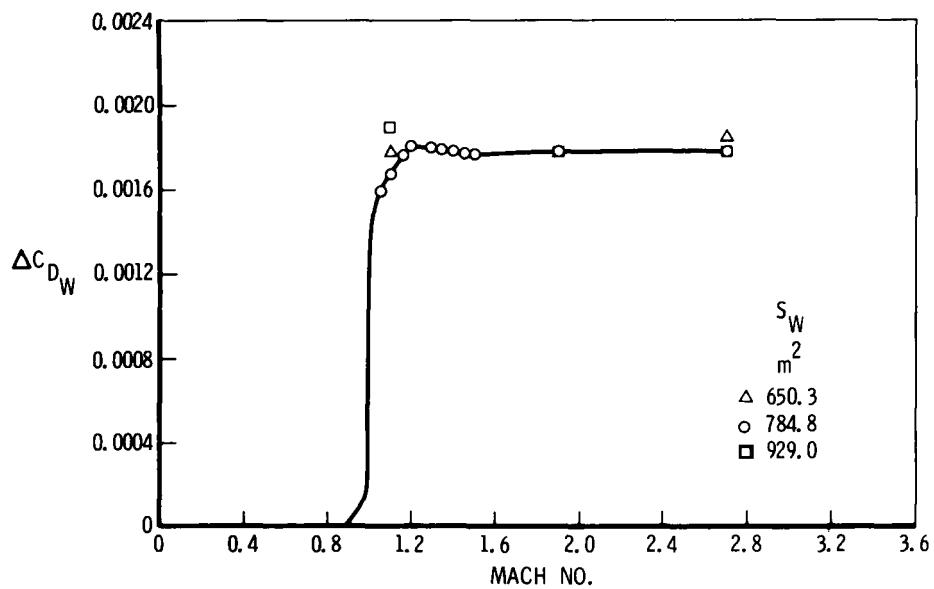


Figure 12.- Blended wing body wave drag.

| $\eta$ | X/C |
|---|---|
| 0.0000 | 0.4 |
| 0.0405 | |
| 0.0788 | 0.4 |
| 0.0835 | 0.4, 0.8 |
| 0.1538 | 0.4 |
| 0.2308 | 0.4 |
| 0.3077 | 0.4 |
| 0.4615 | 0.4 |
| 0.5385 | 0.4 |
| 0.6154 | 0.4 |
| 0.6923 | 0.4 |
| 0.8462 | 0.4 |
| 1.0000 | 0.4, 0.8 |

| $D/Q \ M^2$ | OPT $D/Q \ M^2$ | | $\Delta C_{D_W}$ |
|---|---|---|---|
| 2.652 | 2.521 | (5 $\Theta$) | 0.003212 |
| | 2.409 | (13 $\Theta$) | 0.003070 |

Figure 13.– Wave drag optimization — $M = 2.7$, $C_L = 0.1$, $VOL_{WB} = 1009.9 \ m^3$.



$\eta = 0.0 \ T/C = .065$

$\eta = .0405 \ T/C = .044$

$\eta = .0788 \ T/C = .065$

$\eta = .0835 \ T/C = .025$

$\eta = .1538 \ T/C = .026$

$\eta = .4615 \ T/C = .026$

$\eta = .8464 \ T/C = .026$
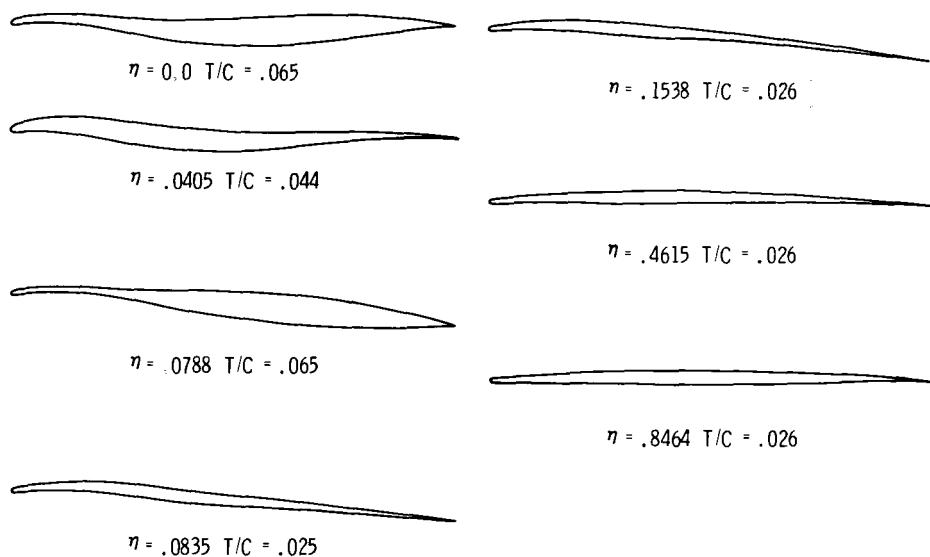
Figure 14.– Sections for minimum wave drag — $C_L = 0.1$.
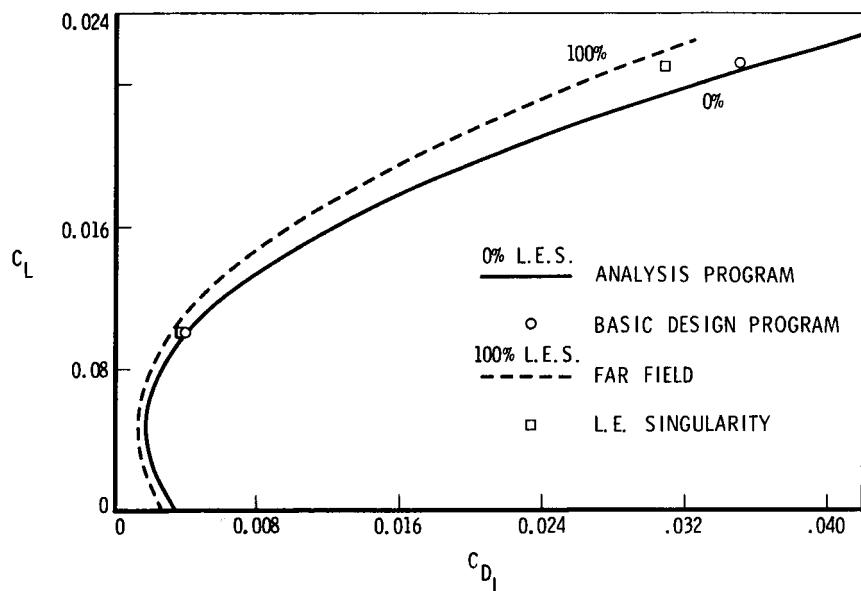
Figure 15.- Trimmed drag due to lift — M = 2.7.
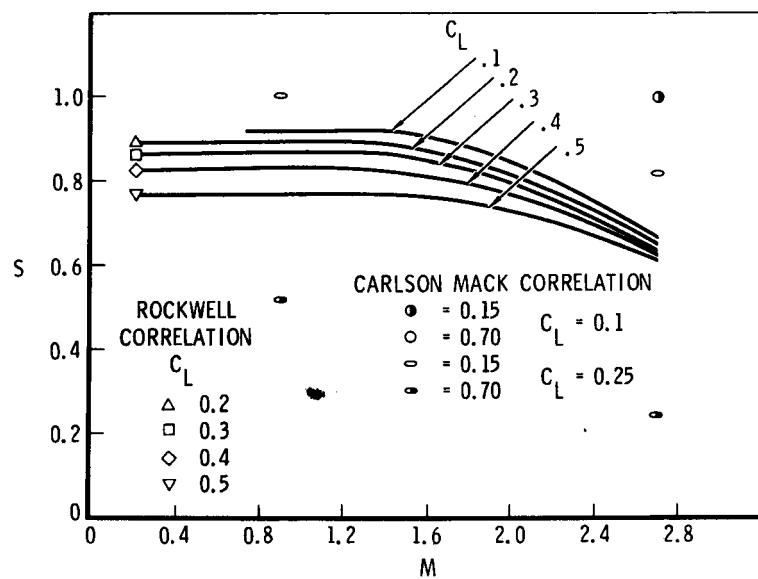


Figure 16.- Leading edge suction parameter.
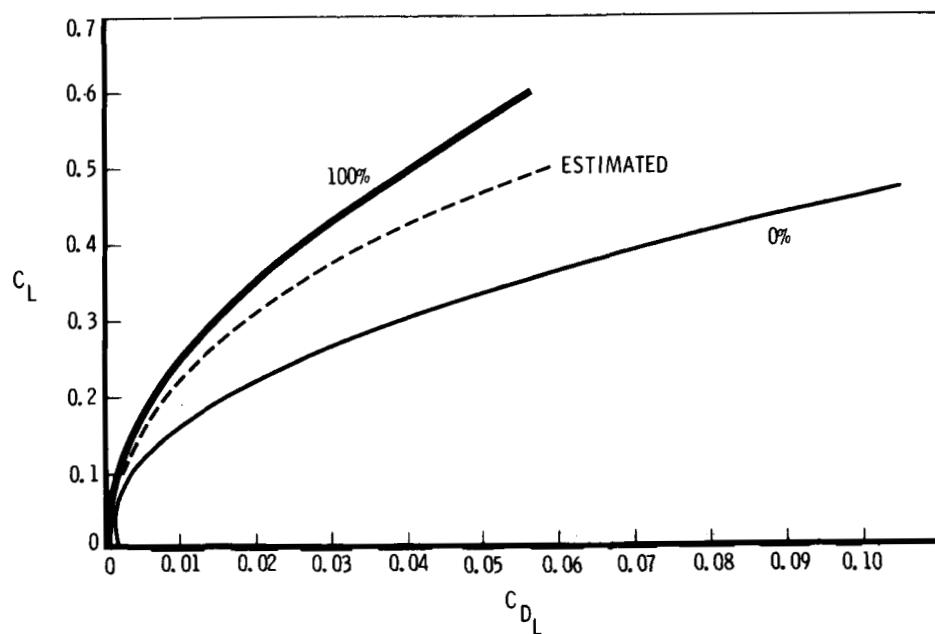
Figure 17.- Trimmed drag due to lift — M = 0.2.
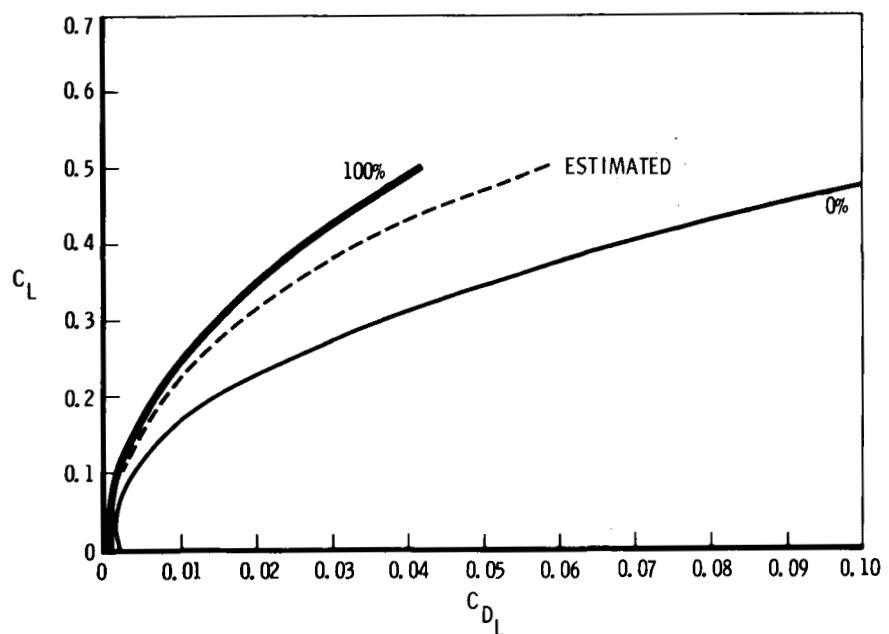


Figure 18.- Trimmed drag due to lift — M = 0.9.
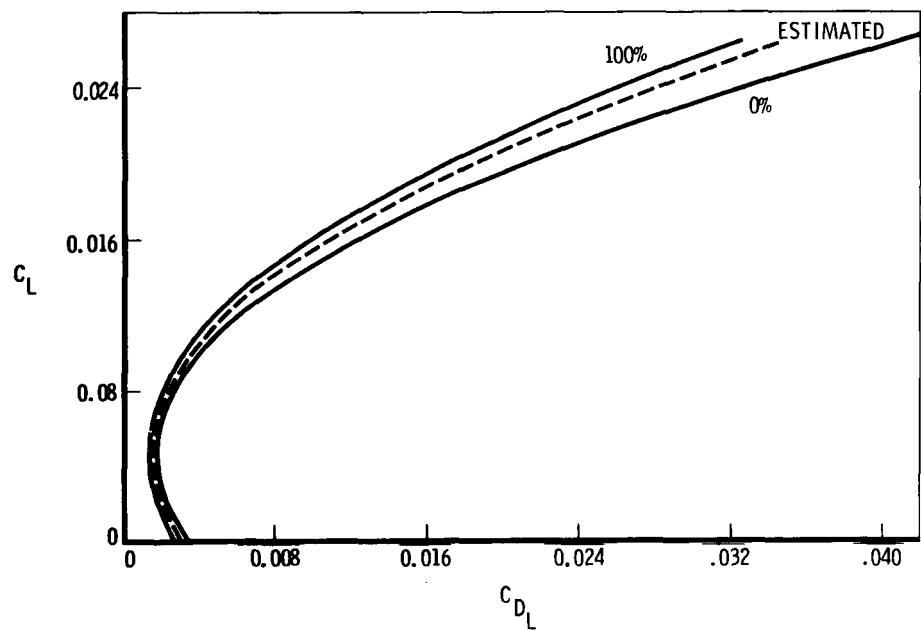
Figure 19.- Trimmed drag due to lift — M = 2.7.
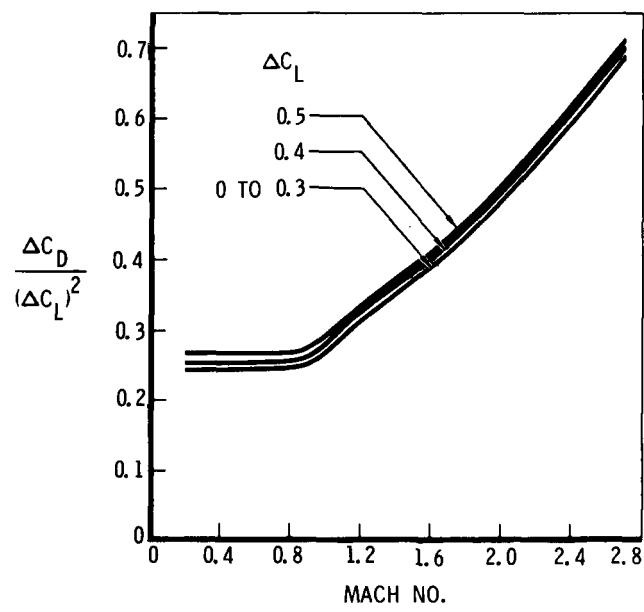


Figure 20.- Trimmed $\Delta C_D/(\Delta C_L)^2$ vs. Mach number.

$$\Delta C_{D_F} \qquad +0.000460$$

$$\Delta C_{D_W} \qquad -0.000186$$

$$\Delta C_{D_L} \qquad +0.000080$$

$$\Delta C_{D_{NAC}} \qquad 0.000354$$

Figure 21.— Nacelle drag increments — $C_L = 0.1$.

| | $c_{D_F}$ | $c_{D_W}$ | $c_{D_L}$ | $c_D$ ROUGH MISC | L/D | |
|---|---|---|---|---|---|---|
| AST 102 | .004440[1] | .002108[1] | .004968[1] | .000 | 8.684 | |
| | .004440[1] | .002108[1] | .004282[2] | .000 | 9.234 | ← |
| | .004358[3] | .002038[3] | .004138[3] | .000261[3] | 9.263 | |
| RB-1 BLENDED WING BODY | .004490 | .001765 | .004146 | .000 | 9.614 | ← |

[1] ROCKWELL ANALYSIS

[2] ROCKWELL TWIST AND CAMBER DESIGN

[3] LTV ANALYSIS ADJUSTED TO M = 2.7

Figure 22.— Zero suction blended wing body design status — M = 2.7, $C_L = 0.1$, $VOL_{WB} = 1139.5 \text{ m}^3$.

| $c_{D_F}$ | $c_{D_{WAVE}}$ | $c_{D_{VORTEX}}$ | LEADING EDGE SUCTION % | (L/D) |
|---|---|---|---|---|
| .004490 | .003070[1] .003101[2] | .001934 | 100 | 10.533 |
| | | | 66 | 10.20 |

| $c_{D_F}$ | $c_{D_{VOLUME\ WAVE}}$ | $c_{D_L}$ | | |
|---|---|---|---|---|
| .004490 | .001773[1] .001760[2] | .004146 | 0 | 9.607 |

[1] LIFTING WAVE DRAG OPTIMIZATION

[2] VOLUME WAVE DRAG OPTIMIZATION

Figure 23.- Blended wing body design status — M = 2.7, $C_L$ = 0.1, $VOL_{WB}$ = 1009.1 m³.
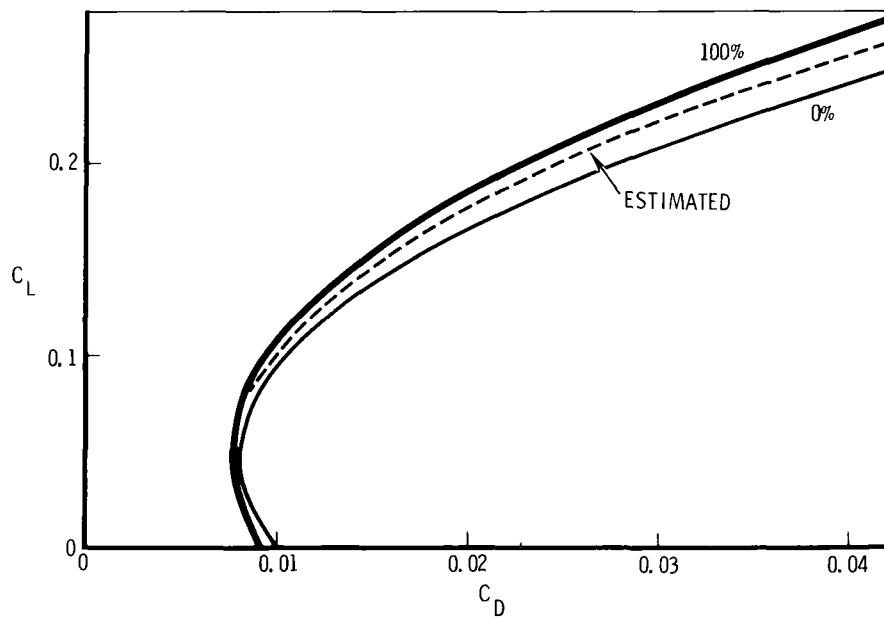


Figure 24.- Trimmed drag polars — M = 2.7.
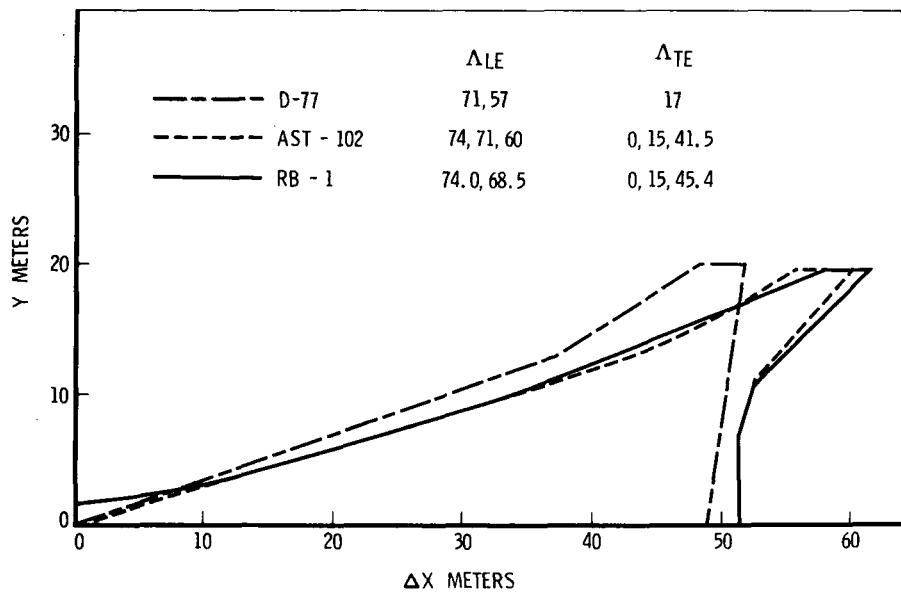
Figure 25.- Planform comparison — M = 2.2.

| | $VOL_{WB}$ $M^3$ | $S_{REF}$ $M^2$ | $c_{D_F}$ | $c_{D_W}$ | $c_{D_L}$ | L/D |
|---|---|---|---|---|---|---|
| D-77 BASELINE | 1103.3 | 873.3 | 0.004710 0.004710 | 0.003032 0.002627** | 0.004600* 0.004108** | 8.102 8.737 |
| AST—102 BASELINE | 1139.5 | 784.8 | 0.004810 | 0.002190 | 0.003410** | 9.597 |
| RB—1 BLENDED WING BODY | 1139.5 | 784.8 | 0.004970 | 0.001780 | 0.003328 | 9.923 |

* WIND TUNNEL MEASUREMENT

** D-77 PLANFORM ROCKWELL DESIGN CODES

Figure 26.- Zero suction blended wing body status — M = 2.2, $C_L = 0.1$.